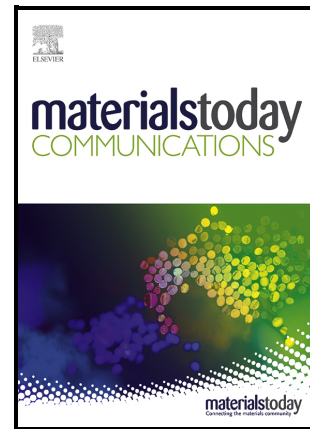


Investigation of speed and temperature effects in mechanical nano-patterning of GaAs via molecular dynamics simulation

Yi Zhang, Jining Sun, Qianhao Xiao, Yunlong Han, Wenbo Zhang, Xichun Luo, Lei Zhang



PII: S2352-4928(24)01345-X

DOI: <https://doi.org/10.1016/j.mtcomm.2024.109364>

Reference: MTCOMM109364

To appear in: *Materials Today Communications*

Received date: 27 March 2024

Revised date: 24 May 2024

Accepted date: 25 May 2024

Please cite this article as: Yi Zhang, Jining Sun, Qianhao Xiao, Yunlong Han, Wenbo Zhang, Xichun Luo and Lei Zhang, Investigation of speed and temperature effects in mechanical nano-patterning of GaAs via molecular dynamics simulation, *Materials Today Communications*, (2024)
doi:<https://doi.org/10.1016/j.mtcomm.2024.109364>

This is a PDF file of an article that has undergone enhancements after acceptance, such as the addition of a cover page and metadata, and formatting for readability, but it is not yet the definitive version of record. This version will undergo additional copyediting, typesetting and review before it is published in its final form, but we are providing this version to give early visibility of the article. Please note that, during the production process, errors may be discovered which could affect the content, and all legal disclaimers that apply to the journal pertain.

Investigation of speed and temperature effects in mechanical nano-patterning of GaAs via molecular dynamics simulation

Yi Zhang¹, Jining Sun^{1,2,*}, Qianhao Xiao^{1,3}, Yunlong Han¹, Wenbo Zhang¹, Xichun Luo³, Lei Zhang^{1,2,*}

¹*School of Mechanical Engineering, Dalian University of Technology, Dalian 116024, China*

²*State Key Laboratory of High-performance Precision Manufacturing, Dalian University of Technology, Dalian 116024, China*

³*Centre for Precision Manufacturing, DMEM, University of Strathclyde, Glasgow G1 1XJ, United Kingdom*

* Corresponding authors.

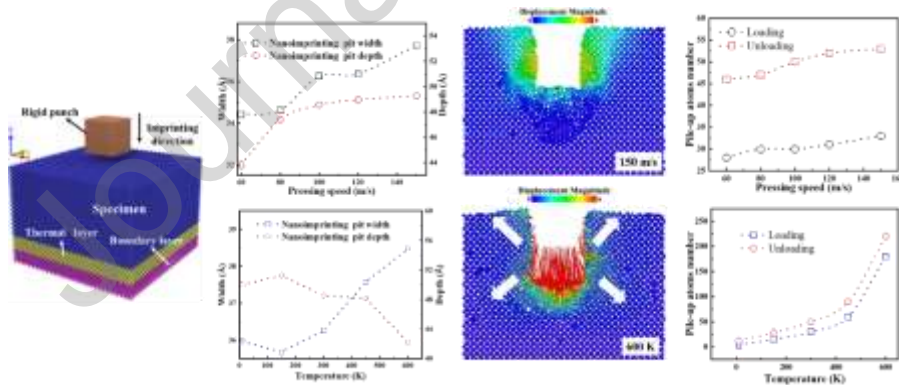
E-mail address: jining.sun@dlut.edu.cn (J. Sun); lei.zhang@dlut.edu.cn (L. Zhang).

ABSTRACT

Speed and temperature are two key parameters governing GaAs mechanical nano-patterning process. For the first time, this study evaluates the effects of pressing speed and nanoimprinting temperature on the deformation behavior and mechanical properties of GaAs in the mechanical nano-patterning process. Simulation results reveal that high pressing speed and high nanoimprinting temperature facilitate the nano-pattern formation on GaAs. For the pressing speed effect, the maximum force, residual stress, and cubic diamond atomic friction

decrease with the elevated pressing speed, while the surface pile-up is minimally influenced by the pressing speed during the nanoimprinting process. Moreover, the morphological accuracy of the nano-patterns is enhanced with increasing pressing speed. For the temperature effect, simulation results reveal that amorphization and plastic activity exhibit a positive correlation with increasing nanoimprinting temperature, whereas the maximum force and residual stress demonstrate a roughly inverse relationship with nanoimprinting temperature. Additionally, the elevated temperature also exerts a substantial influence on the dislocation density, morphological accuracy, and surface pile-up. This study contributes to a comprehensive understanding of the effects of these two key factors on the mechanical properties and deformation behavior of GaAs in mechanical nano-patterning.

Graphical abstract



Keywords: Nano-patterning; GaAs; Residual stress; Deformation behavior; Molecular dynamics

1. Introduction

Nano-patterned single-crystal GaAs is widely used in solar panels [1,2], nanophonics [3,4], and high-speed semiconductor devices [5,6], owing to its high electron migration rate and direct bandgap. The nanoimprinting technique is a highly-throughput, cost-effective, and user-friendly method [7–9] for direct mechanical nano-patterning over a large area. It employs a rigid mold to achieve precise manipulation of materials through controlled mechanical deformation under specific temperature and pressure conditions [10]. Over the past few decades, this simple mechanical machining method has been developed for a variety of applications such as nanofluid devices, nanoelectronics, and high-density data storage systems [7,9]. The nanoimprinting technique was initially developed for imprinting on soft polymers. However, recent advancements have demonstrated its feasibility in direct nanoimprinting on hard materials [11–13]. Given that the substrate material undergoes deformation in the nanoimprinting process to generate nano-patterns, comprehending the deformation mechanism is of utmost importance.

Numerous studies have investigated the deformation mechanism during the nanoimprinting process by utilizing the molecular dynamics (MD) simulation, thereby offering preliminary insights into tooling design and determination of nanoimprinting conditions [14–16]. Wang et al. [17] investigated the mechanical behavior of amorphous Ni-Zr alloys during the nanoimprinting process. They observed that the hardness and modulus of amorphous Ni-Zr alloy increase proportionally with an elevated concentration of Zr atoms. Moreover, the pile-up index exhibited a positive correlation with nanoimprinting temperature. The effects of punch shape and adhesive energy on the nanoimprinting process were investigated by Kang et al. [18]. Nguyen et al. [19] revealed that an increase in vibration

frequency leads to an augmentation in groove depth. Moreover, the groove shape could be significantly influenced by factors such as punch angle, nanoimprinting temperature, and vibration factor. Besides, the mechanical behaviors of Cu-Ni alloys, which were nanoimprinted and annealed, were also investigated through MD simulations by Fang et al. [20]. Park et al. [21] demonstrated that elevating the substrate temperature can effectively enhance the demolding process. Koyama et al. [22] conducted a comprehensive investigation on the impact of punch size and shape on the nanoimprinting process. The imprinting force, plastic deformation, and dislocation movement in the nanoimprinting process of copper with a diamond punch were investigated by Pei et al. [23]. Zhu et al. [24] proposed a two-step precision glass molding technique for the fabrication of micro-nano structure arrays with antireflective properties on chalcogenide glass under a constant molding temperature of 307 K. Riyadi et al [25] studied the effects of mold geometry and imprinting temperature on the quality of metallic glass films. Pham et al [26] conducted the nanoimprinting process using a punch with an angle of 0° to imprint FeNiCoCrCu high-entropy alloys via MD simulation. They revealed that the imprint force increased with the increasing imprint speed.

The above studies are mainly focused on the deformation mechanism exhibited by ductile materials under different nanoimprinting conditions. Conversely, the deformation mechanism of hard-brittle materials may significantly differ from that of ductile materials due to the differentiation in atomic bonding types [27]. However, the underlying mechanism of the deformation response of GaAs during the nanoimprinting process is still scarce. Meanwhile, considering that the optimization of mechanical nano-patterning quality relies on the manipulation of pressing speed and nanoimprinting temperature, this study aims to

comprehensively investigate the impact of these factors on the formation process of nano-patterns during nanoimprinting. Specifically, the nanoimprinting will be conducted using large-scale MD simulations at various pressing speeds, ranging from 60 m/s to 150 m/s, and nanoimprinting temperature variations spanning from 10 K to 600 K. Attention is focused on the effects of the above factors on the atomic deformation behavior, mechanical response, surface pile-up, and morphological accuracy in the nano-patterns machining process.

2. Methodology

2.1. MD simulation

The MD simulations in this study were performed using the Open-source LAMMPS package, developed by Plimpton [28]. The nanoimprinting MD model consists of a diamond cubic punch, GaAs specimen, boundary layer, and thermal layer as shown in **Fig. 1**. Considering the primary focus of this research on investigating the impact of nanoimprinting temperature and pressing speed on GaAs specimen deformation during the nanoimprinting process, a simplified cubic punch shape was adopted for ease of analysis [20]. The cubic diamond punch can be considered as a rigid body owing to its significantly higher hardness in comparison with the GaAs specimen. It should be noted that the lattice arrangement of perfect monocrystal GaAs follows the diamond structure [29,30]. The size of the specimen is $30a_0 \times 30a_0 \times 21a_0$, where a_0 is the lattice constant (5.653 Å). The diamond punch and specimen consisted of 11,650 atoms and 153,000 atoms, respectively. To ensure the structural stability of specimen atoms throughout the nanoimprinting process, the lowest bottom layer was held in a fixed position. The thermostatic layer functions as a temperature mediator, establishing a

thermal linkage between the atoms in the specimen layer and the surrounding environment, thereby maintaining the specimen layer at a predetermined temperature. The motion of atoms in the thermostatic and specimen layers adheres to Newton's second law, while the Velocity-Verlet algorithm is employed with a time step of 1 fs for integrating the Hamiltonian equations of motion. Before the nanoimprinting process, the energy of the GaAs specimen was minimized using the conjugate gradient method to adjust atom coordinates [31]. In addition, the punch was positioned at 10 Å from the surface of the GaAs specimen, with its movement aligned along the negative direction of the Z-axis. The X- and Y-directions are subject to periodic boundary conditions (P. B. C), whereas the Z-direction exhibits non-periodicity (n-P. B. C) [32].

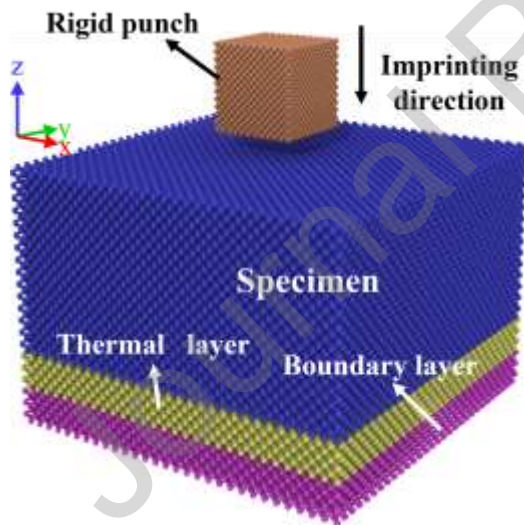


Fig. 1. Schematic illustration of nanoimprinting simulation model.

During the nanoimprinting process, five different pressing speeds (60 m/s, 80 m/s, 100 m/s, 120 m/s, and 150 m/s) were applied. Prior to nanoimprinting, the desired temperature of the Newton layer atoms and thermal layer atoms (10 K, 150 K, 300 K, 450 K, and 600 K) was achieved by equilibrating the sample for about 30 ps by employing a fast and robust Nose-

Hoover method [33]. During the nanoimprinting process, adherence to Newton's second law was observed in the Newton layer atoms while heat generated by these atoms was efficiently dissipated through the thermal layer via the Nose-Hoover method to maintain a constant temperature within the Newton layer. The temperatures below 300 K were referred to as low temperature (LT), while temperatures more than 300 K were denoted as high temperature (HT). The nanoimprinting process can be separated into the following three stages: the pressing stage, the stay stage, and the demolding stage. After the pressing stage, the punch was retained in the specimen for a duration of 30 ps, followed by demolding at a speed of 100 m/s.

2.2. Calculation and visualization analysis

The potential function system in the simulation involved atomic interactions between the GaAs specimen atoms, the interactions between the punch atoms, and the interactions between the specimen and the punch atoms. The specific forms of the atomic interactions have been elucidated in prior publications [34–36]. The open visualization tool (OVITO software) [37] was used to conduct visualization and analysis of the simulation results. The post-processing methods included the dislocation extraction algorithm (DXA) [38,39], von Mises (VM) stress calculation [40,41], and atomic displacement calculation [42].

The von Mises stress comprehensively accounts for the combined effects of all six stress components and has been extensively utilized to quantitatively characterize residual stress [43,44]. The VM stress was computed utilizing the atomic stress tensor, as depicted in **Eq. (1)**.

$$\sigma_{VM} = \sqrt{\frac{6\tau_{xy}^2 + 6\tau_{yz}^2 + 6\tau_{xz}^2 + (\sigma_{xx} - \sigma_{yy})^2 + (\sigma_{xx} - \sigma_{zz})^2 + (\sigma_{zz} - \sigma_{yy})^2}{2}} \quad (1)$$

where τ_{xz} , τ_{yz} , τ_{xy} , σ_{yy} , σ_{xx} , and σ_{zz} are six components of the atomic stress tensor. In addition, the calculation of η_i^{Mises} for each atom according to their local von Mises shear invariant was adopted to quantify plastic deformation at atomic scale [45], as shown in **Eq. (2)**.

$$\eta_i^{Mises} = \sqrt{\frac{6\eta_{xy}^2 + 6\eta_{yz}^2 + 6\eta_{xz}^2 + (\eta_{xx} - \eta_{yy})^2 + (\eta_{xx} - \eta_{zz})^2 + (\eta_{zz} - \eta_{yy})^2}{6}} \quad (2)$$

where η_{xz} , η_{yz} , η_{xy} , η_{yy} , η_{xx} , and η_{zz} are six components of the atomic strain tensor. The hardness of a material is determined by the maximum load P_{max} and the projected contact area A_c , which can be quantified using the Oliver-Pharr method [46], as shown in **Eq. (3)**.

$$H = \frac{P_{max}}{A_c} \quad (3)$$

3. Results and discussion

3.1. Effects of pressing speed on nanoimprint mechanical properties and atomic displacement

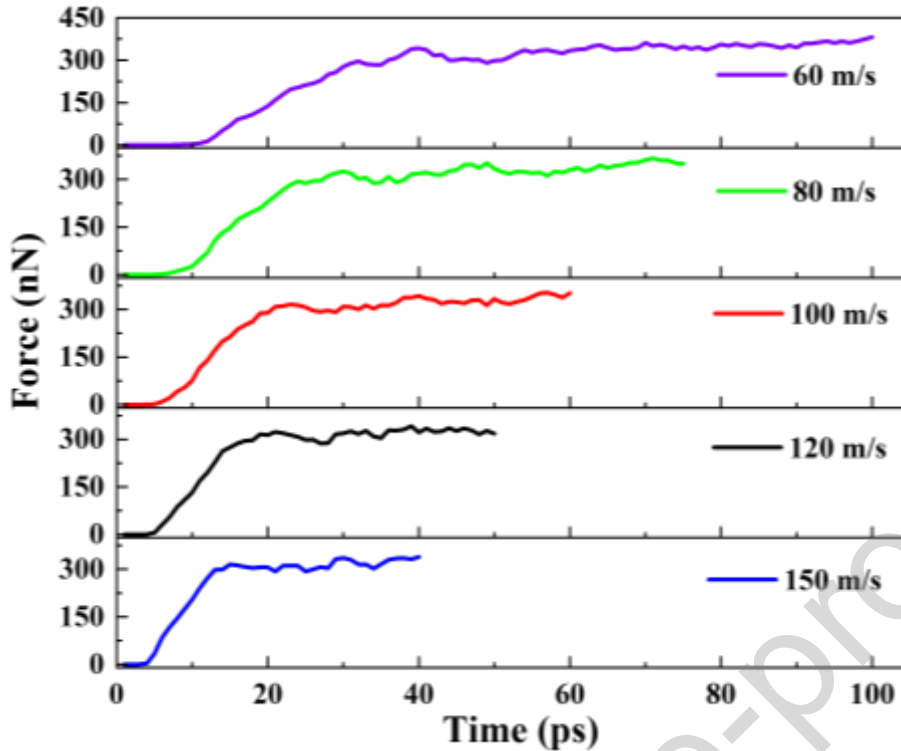


Fig. 2. Effect of different speeds on the pressing force responses of GaAs specimens at a nanoimprinting temperature of 300 K.

The pressing force response of the GaAs specimen at the chosen pressing speed during the pressing stage is depicted in **Fig. 2**. The results show that the maximum pressing forces for the pressing speed of 60 m/s, 80 m/s, 100 m/s, 120 m/s, and 150 m/s are 381 nN, 367 nN, 352 nN, 341 nN, and 338 nN, respectively, as shown in **Fig. 3(a)**. Surprisingly, a negative correlation between the maximum pressing force and the pressing speed is observed in **Fig. 3(a)**, which is substantially different from that of ductile materials as has been reported in previous studies [47–49]. Meanwhile, the fraction of cubic diamond atoms below the punch at various pressing speeds is shown in **Fig. 3(b)**. It can be observed that the diamond atomic fraction decreases with an increase in pressing speed. The result depicted in **Fig. 3(c)** illustrates a decrease in the average von Mises stress with an increase in pressing speed, indicating a negative correlation between residual stress and pressing speed. Moreover, the

pressing speed exerts negligible influence on the surface pile-up, as shown in **Fig. 3(d)**.

The negative correlation between the maximum pressing force and the pressing speed arises from the fact that the higher pressing speed leads to the appearance of higher strain energy and activated shear transformation zones (see **Fig. 4(c₁)**) within GaAs, creating an increasing number of dislocations (as shown in **Fig. 4(c₂)**) and structural defects (see **Fig. 3(b)**), and thereby in turn decreases the mechanical stiffness of the GaAs specimen. The negative correlation between the pressing speed and the maximum pressing force is analogous to that discovered in monocrystalline silicon [50]. The increasing in imprinting pressing speed (from 60 m/s to 150 m/s) leads to an augmentation of atomic shear strain at the lateral sides of the punch, as depicted in **Fig. 4(a₁)–(c₁)**. Consequently, the resulting free volume caused by shear band at higher pressing speed does not propagate towards the surface. Therefore, altering the pressing speed has a negligible impact on surface pile-up.

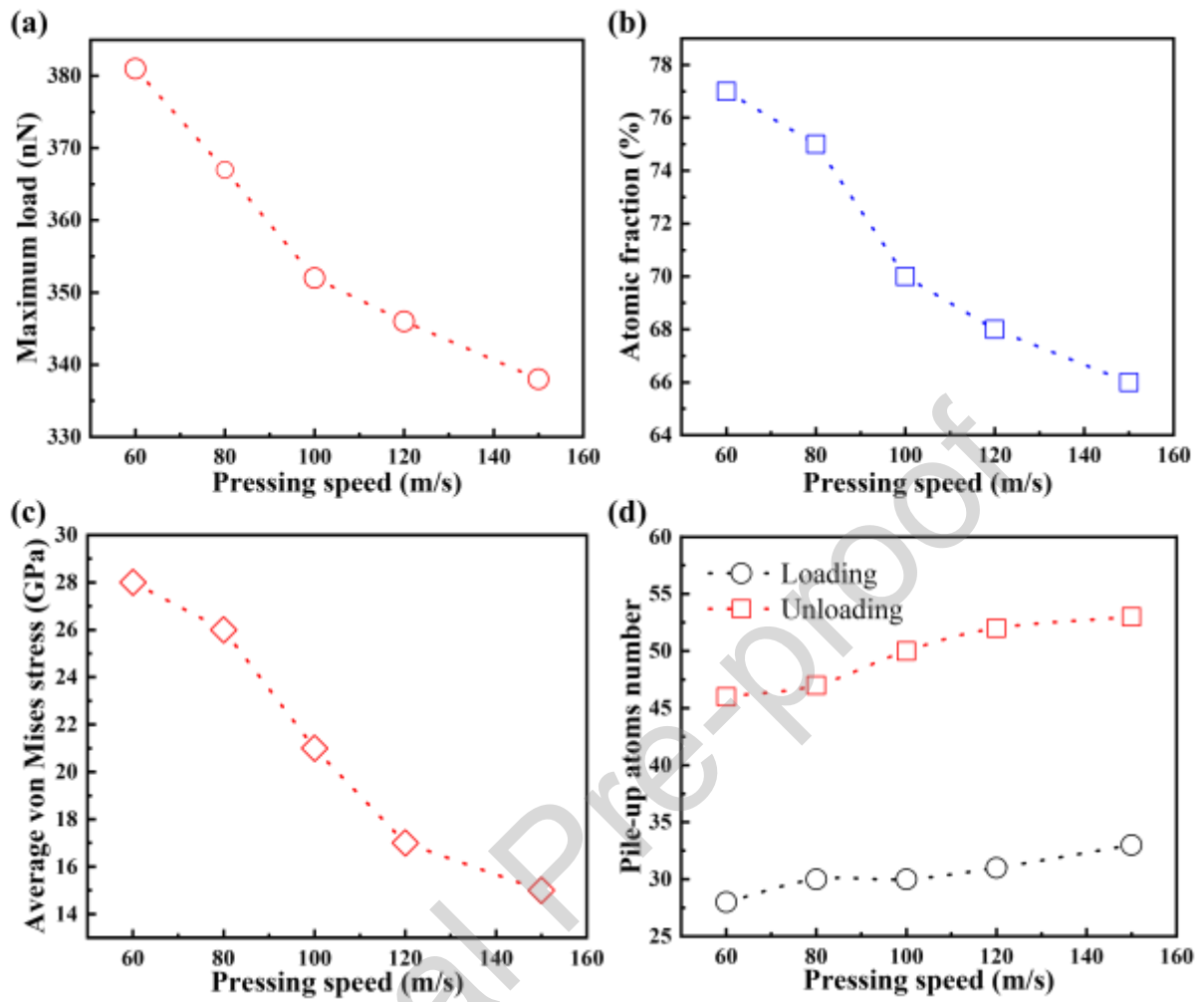


Fig. 3. Effect of different pressing speeds on mechanical response and surface pile-up of imprinted GaAs specimen: (a) maximum pressing force, (b) the cubic diamond atomic fraction, (c) average von Mises stress, and (d) surface pile-up atoms.

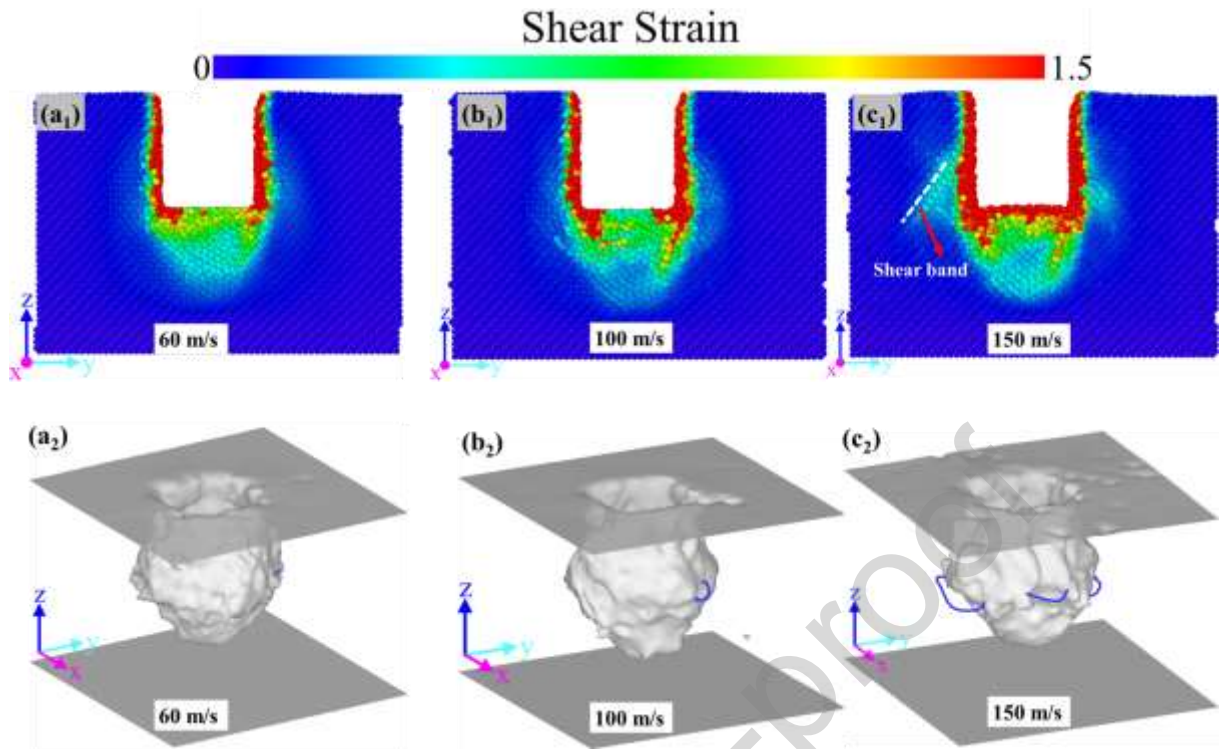


Fig. 4. Distribution of atomic shear strain (from (a₁) to (c₁)) and dislocations (from (a₂) to (c₂)) of GaAs specimens at a pressing speed of (a) 60 m/s, (b) 100 m/s, and (c) 150m/s.

Since the shape of the nanoimprinted pit is rectangular, the effects of pressing speed on morphological accuracy are investigated by measuring the width and depth of the pit. **Fig. 5** exhibits the atomic displacement distribution and pit morphological accuracy for the various pressing speeds after demolding. The results demonstrate that the geometry of the imprinted nano-patterns is more consistent with the shape of the punch at high pressing speed. Moreover, the morphological accuracy exhibits positive pressing speed-dependent, primarily attributed to the suppression of elastic recovery at high pressing speeds.

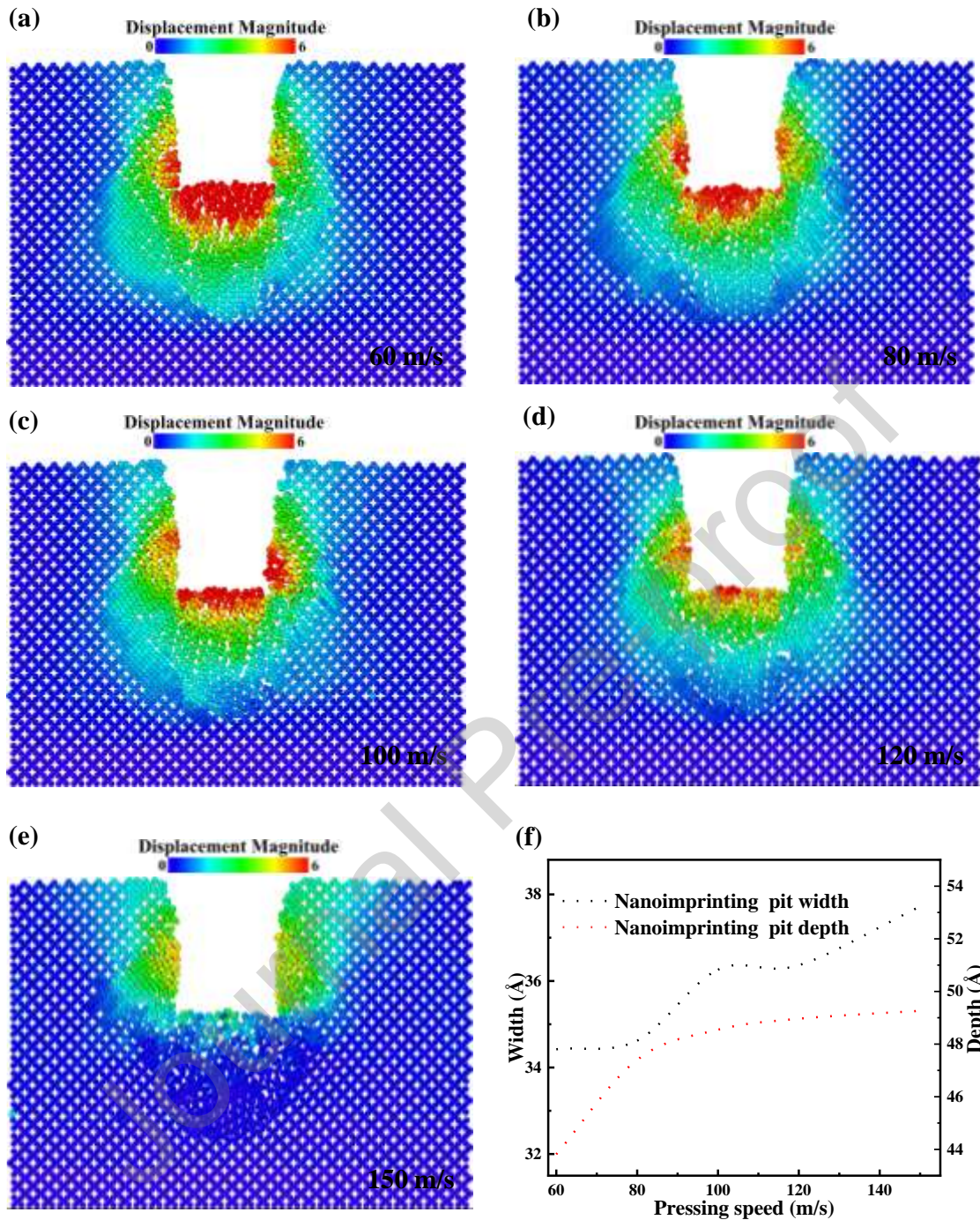


Fig. 5. The atomic displacement distribution after demolding at a pressing speed of (a) 60 m/s, (b) 80 m/s, (c) 100 m/s, (d) 120 m/s, and (e) 150 m/s. The width and depth of the nanoimprinting pit after demolding at different pressing speeds are shown in (f).

3.2. Effect of nanoimprinting temperature on plastic deformation behavior

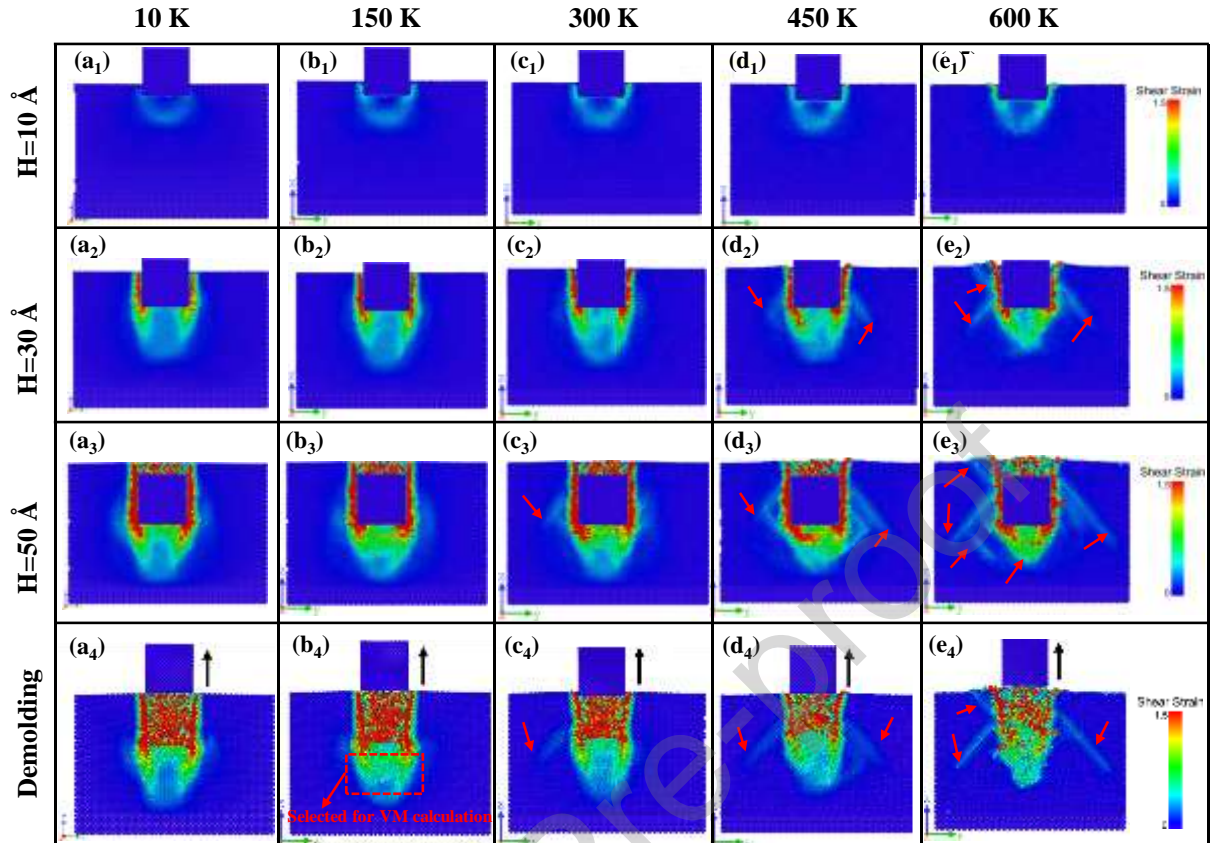


Fig. 6. Distribution of atomic shear strain of GaAs specimens vs. nanoimprinting temperature at different depths of nanoimprinting: (a₁)–(e₁) 10 Å, (a₂)–(e₂) 30 Å, (a₃)–(e₃) 50 Å. The distribution of atomic shear strain after demolding is shown in (a₄)–(e₄). The white dashed line denotes the position of the shear band.

The nanoscale plastic deformation behavior is related to the mechanical response and morphological accuracy of the nanoimprinting pattern. Hence, it is necessary to study the nanoimprinting temperature effects on atomic deformation behavior during the nanoimprinting process. According to **Eq. (2)**, it is evident that the atomic shear strain can serve as a quantitative measurement for characterizing plastic deformation at the atomic level.

Fig. 6(a)–(e) displays the atomic shear strain magnitude of GaAs specimen during the nanoimprinting process at 10 K, 150 K, 300 K, 450 K, and 600 K, respectively. Regardless of the specimen temperature, the plastic deformation region mainly extends along the z direction

when the nanoimprinting depth is less than 10 Å, as depicted in **Fig. 6(a₁)–(e₁)**. This indicates the atomic plastic deformation is minimally influenced by temperature at lower depths of nanoimprinting. However, the influence of temperature on the atomic plastic deformation becomes significantly pronounced when the nanoimprinting depth exceeds 30 Å. Specifically, two small V-shaped shear strain regions can be observed primarily below the punch when nanoimprinting at LT, as depicted in **Fig 6(a₂)–(c₂)**. In contrast, the GaAs substrate exhibits a significant atomic plastic deformation, as evidenced by a pronounced V-shaped shear strain below the punch and shear band (SB) at the lateral direction of the punch when nanoimprinting at HT, as shown in **Fig. 6(d₂)** and **Fig. 2(e₂)**. Moreover, the distribution of atomic shear strain and shear bands at 50 Å exhibits a resemblance to that observed at 30 Å, as depicted in **Fig 6(a₃)–(e₃)**. It should be noted that the shear bands can facilitate the flow of plastic deformation and create densification [51] around the punch, as shown in **Fig. 6(e₂)** and **Fig. 6(e₃)**. It is known that the density in the surroundings of an SB is significantly increased [52,53]. The strain densification is enhanced at HT due to the presence of a greater number of shear bands and the accumulation of free volume within the GaAs specimen. The occurrence of shear bands facilitates plastic deformation, while strain densification helps maintain pressure stability during this process [51]. Given the correlation between strain densification and SB, as well as the effect of nanoimprint temperature and pressing speed on SB formation, it becomes crucial to enhance the quality of nanoimprinting by carefully selecting appropriate parameters (temperature or speed) that either prevent SB formation or facilitate its elimination after demolding. Besides, the shear bands occur mostly along the direction of $[0\bar{1}\bar{1}]$ or $[01\bar{1}]$, which is oriented at a 45°

angle relative to the punch loading direction, consistently aligning with GaAs's cleavage fracture [54]. In summary, the elevated nanoimprinting temperature can facilitate the densification and plastic deformation in the surroundings of the punch through shear bands and increased shear strain.

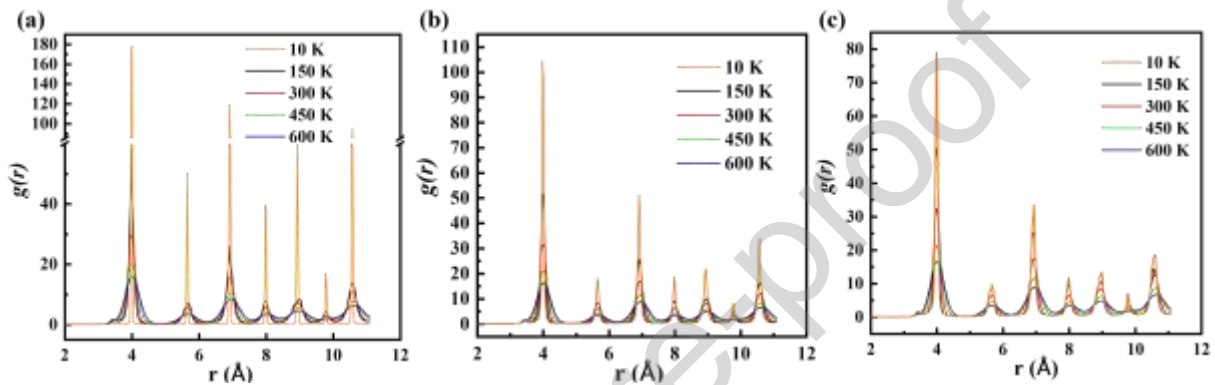


Fig. 7. The RDF diagrams of GaAs specimens with different nanoimprinting temperatures at the depth of: (a) 10 Å, (b) 30 Å, and (c) 50 Å.

Additionally, **Fig. 6(a₄)–(e₄)** demonstrates distinct variations in the atomic shear strain of the GaAs specimen after demolding. The elevated nanoimprinting temperatures can enhance atomic motion, leading to a pronounced elastic recovery of the atomic shear strain at HT. Specifically, as shown in **Fig. 6(d₄)** and **Fig. 6(e₄)**, the demolding results in the elimination of the shear bands below the pit, indicating a significant elastic recovery of the damaged subsurface structure. Conversely, as depicted in **Fig. 6(a₄)–(c₄)**, the elastic recovery of specimen atoms is hindered at LT, resulting in a significant residual shear strain and minimal elastic recovery.

Furthermore, the degree of the structural deformation is quantified using the radial distribution function (RDF) [55]. The $g(r)$ curves of the GaAs specimen at different

nanoimprinting temperatures under the nanoimprinting depth of 10 Å, 30 Å, and 50 Å are shown in **Fig 7**. The peak height of $g(r)$ exhibits a discernible decline, whereas the peak width shows an augmentation as the substrate temperature increases, implying intensified atomic vibrations and increased atom displacements. Moreover, an increase in the depth of nanoimprinting leads to a corresponding reduction in the intensity of the peak. The findings suggest a substantial enhancement in plasticity with increasing nanoimprinting temperature, resulting in a more pronounced amorphous state during the nanoimprinting process.

3.3. Effect of nanoimprinting temperature on mechanical response

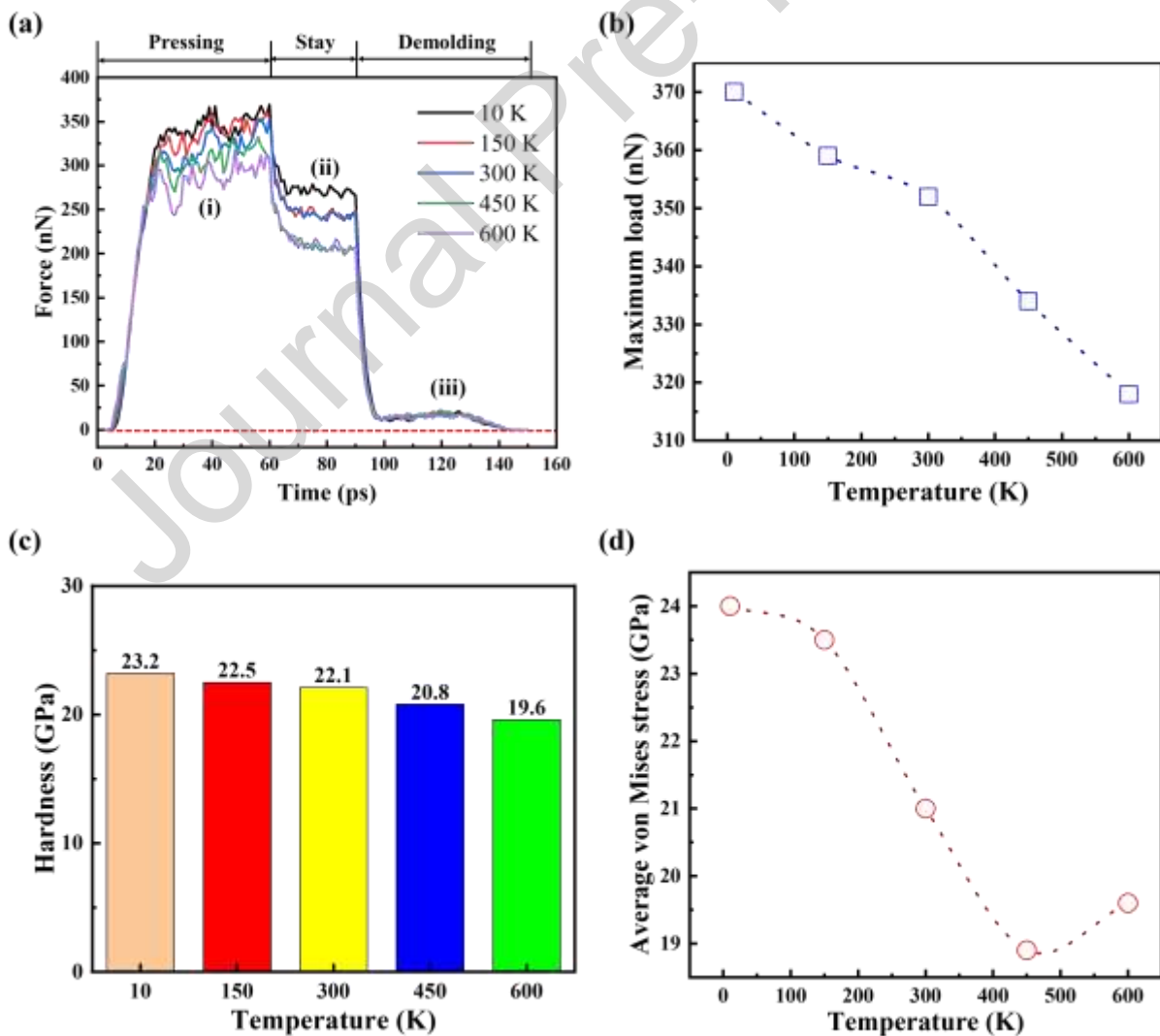


Fig. 8. The mechanical response of GaAs specimen at different nanoimprinting temperatures during the nanoimprinting process: (a) pressing force, (b) maximum pressing force obtained from (a), (c) the maximum hardness, and (d) average von Mises stress. The region for calculating the average von Mises stress in (d) is determined by the red box shown in **Fig. 6(b4)**.

Given that the nanoimprinting technique relies on the direct mechanical deformation of materials, it is imperative to investigate the mechanical response of GaAs at various nanoimprinting temperatures. The variations of force with time for different nanoimprinting temperatures during the nanoimprinting process are illustrated in **Fig. 8(a)**. The force curves can generally be divided into three stages of the nanoimprinting process: (i) pressing (0–60 ps), (ii) stay (60–90 ps), and (iii) demolding (90–150 ps). Simulation results reveal that the pressing force significantly increases at a time of 0–20 ps (corresponding to $h < 10 \text{ \AA}$), followed by large fluctuations from 20 ps to 60 ps ($10 < h < 50 \text{ \AA}$). The fluctuations of pressing force (from 20 ps to 60 ps) are closely associated with the plastic deformation of the GaAs specimen, which primarily encompasses two fundamental forms: structural phase transition and dislocation slip. **Fig. 9** illustrates the structural phase transition during the plastic deformation stage at three distinct temperatures (10K, 300K, and 600K). It can be observed that as the imprinting depth increases, the region of structural phase transition not only emerges beneath the punch but also extends throughout the entire interior of the specimen. This phenomenon becomes more pronounced at high-temperature nanoimprinting. Furthermore, **Fig. 12(b)** (see **section 3.4**) demonstrates that regardless of nanoimprinting temperature, there are dynamic variations in dislocation density during the nanoimprinting process. Consequently, both structural phase transitions and dislocation evolution contribute

to fluctuations in pressing force.

Subsequently, the force curves demonstrate a sudden decline followed by subsequent minor fluctuations during the stay time ($h = 50 \text{ \AA}$), which are associated with the atomic readjustments required to relax the accumulated strain energy of the specimen. Finally, during the demolding stage, the pressing force initially undergoes a rapid decline, followed by a slight reduction due to specimen recovery and interfacial friction between the punch and side wall of the nanoimprinting pit. The maximum loading force and hardness exhibit temperature-dependent variations, as illustrated in **Fig. 8(b)** and **Fig. 8(c)**. According to the previous analysis, the strain densification around the punch at HT would cause high stresses at the plastic deformation region. However, with increasing temperature, the interatomic distance exhibits an expansion while the covalent bond energy of specimen atoms decreases, consequently resulting in a reduction in maximum load force and hardness. Hence, the influence of thermal softening on mechanical response outweighs that of strain hardening. The variation in loading force with temperature exhibits a resemblance to that observed in other semiconductor materials, such as gallium nitride [56] and silicon [57].

Furthermore, the plastic recovery of the imprinted nano-pattern is primarily attributed to residual stress, necessitating a reduction in residual stress after demolding. The residual stress is influenced by both the pressing force and the subsequent elastic recovery. **Fig. 8(d)** illustrates the temperature-dependent residual stress curves of the chosen area from **Fig. 6(b₄)**, which corresponds to the primary damage area. As shown in **Fig. 8(d)**, the average residual stress slightly decreases with the temperature from 10 K to 150 K, then it dramatically decreases and reaches its minimum value at 450 K, and then increases with further increasing

the specimen temperature to 600 K.

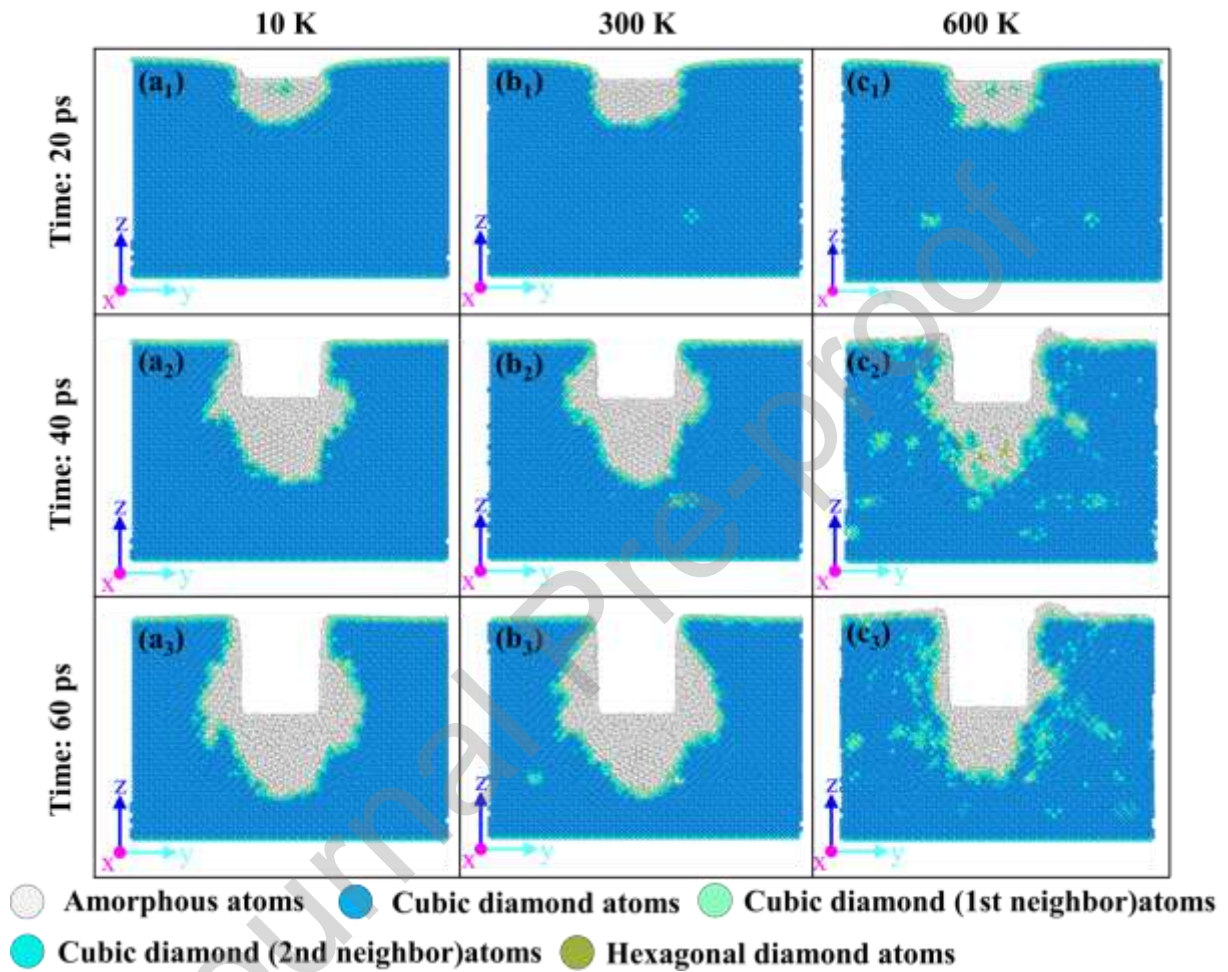


Fig. 9. Structure change of GaAs specimens under nanoimprinting at various temperatures.

3.4. Effect of nanoimprinting temperature on surface pile-up and morphological accuracy

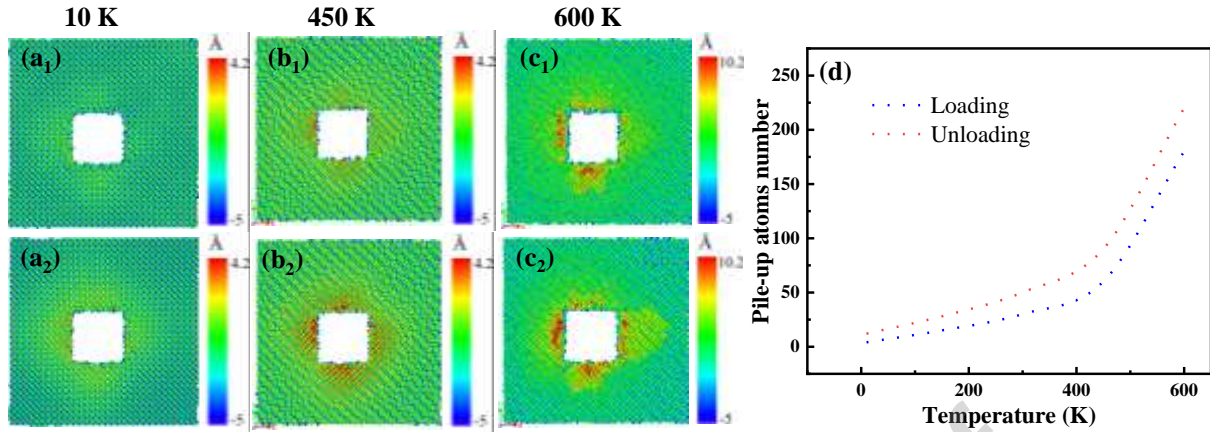


Fig. 10. Surface pile-up snapshots vs. nanoimprinting temperature before demolding of (a₁)–(c₁) and after demolding of (a₂)–(c₂). The number of surface pile-up atoms vs. nanoimprinting temperature is shown in (d).

The snapshots of surface pile-up before and after demolding under different nanoimprinting temperatures (10 K, 450 K, and 600 K) are depicted in **Fig. 10(a₁)–(c₁)** and **Fig. 10(a₂)–(c₂)**, respectively. **Fig. 10(d)** illustrates the number of pile-up atoms vs. specimen nanoimprinting temperature. It can be observed that the surface pile-up decreases 97.8% from 180 (600 K) to 4 (10 K) before demolding. The increase in pile-up can be attributed to two primary factors. Firstly, the extension of the shear band towards the surface creates a channel for the plasticity to flow that induces the formation of pile-up on the surface. Secondly, the temperature-dependent variation in atomic motion direction contributes to the observed disparity in surface accumulation. Specifically, during the pressing stage at HT (e.g., 600 K, refer to **Fig. 11(b)**), there is an enhanced propensity for atomic migration towards the surface at lateral sides of the punch compared to LT (e.g., 10 K, refer to **Fig. 11(a)**), increasing surface pile-up. In addition, the increased surface pile-up observed after demolding can be attributed to the interfacial friction between the punch and the sidewall of the nanoimprinting pit. In summary, the combined influence of shear bands, temperature-dependent atomic

movement, and interfacial friction between the punch and nano-pattern at HT is more likely to result in a rougher morphology on the GaAs surface.

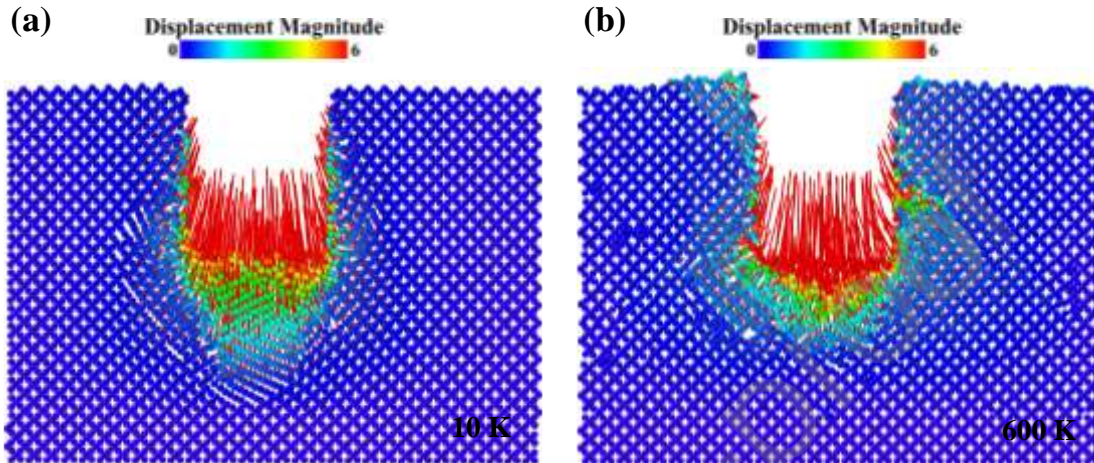


Fig. 11. Atomic displacement vectors map at nanoimprinting depth of 50 Å vs. nanoimprinting temperature: (a) 10 K and (b) 600 K.

After demolding, the nanoimprinted pattern would elastically rebound and significantly affect the accuracy of the nanoimprinted feature. As shown in **Fig. 12(a)**, the pit width decreases with increasing the nanoimprinting temperature, and the lowest width can be found at 150 K. After that, the pit width would significantly increase with further increasing the nanoimprinting temperature to 600 K. In contrast, the pit depth initially increases with increasing the nanoimprinting temperature from 10 K to 150 K, then significantly decreases with the elevated nanoimprinting temperature. It is worth noting that the inflection point (at 150 K) in the pit depth or width curve could be attributed to a higher dislocation density occurring at 150 K (refer to **Fig. 12(b)**) during the nanoimprinting process, resulting in a non-monotonic change in elastic recovery or plastic deformation with the elevated temperature. Overall, at the nanoimprinting temperatures of 10 K, 150 K, 300 K, and 600 K, the pit depth

or width suffers from a significant elastic recovery. Meanwhile, at the nanoimprinting temperature of 450 K, the higher dislocation density enhances plastic deformation and diminishes the elastically rebound of the specimen. In comparison, the best morphological accuracy can be obtained at the nanoimprinting temperature of 450 K.

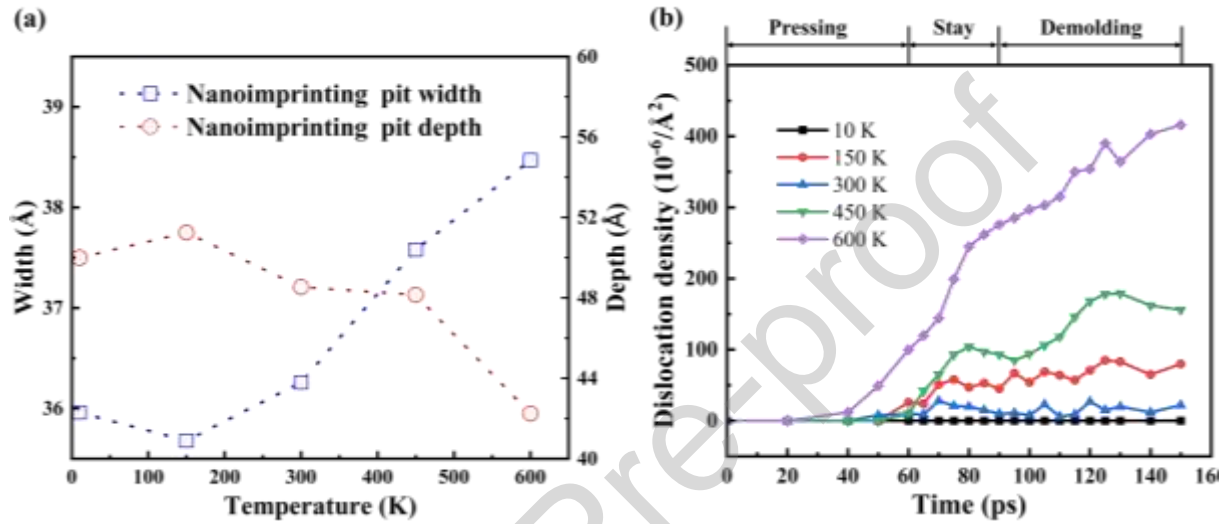


Fig. 12. The width and depth of the nanoimprinting pit vs. nanoimprinting temperature after demolding are shown in (a). The variations of dislocation density in the formation of the nanoimprinting pit during the nanoimprinting process under different nanoimprinting temperatures for GaAs specimens are plotted in (b).

4. Conclusions

For the first time, this study focuses on the effects of pressing speed and nanoimprinting temperature on the mechanical nano-patterning of GaAs specimens by utilizing a simplified cubic punch via MD simulations. Based on the results and discussions, the main conclusions are drawn as follows.

- (1) High-speed pressing leads to a thermal softening effect at the contact area. As the increasing of the pressing speed, the maximum force and diamond atomic fraction

decrease. This result indicates that nano-patterns on GaAs substrate are more easily formed under high-speed pressing, which is in contradiction with the general understanding of ductile materials.

- (2) It is found that the elastic recovery effect can be suppressed at high pressing speeds. The geometry of the imprinted nano-patterns is therefore more consistent with the shape of the punch at high pressing speed, and the shape morphological accuracy is also improved under such conditions.
- (3) The atomic shear strain, shear bands, and dislocation density all increase with the nanoimprinting temperature. Therefore, high-temperature nanoimprinting facilitates the nano-pattern formation process in a ductile regime.
- (4) Both the geometry and geometry accuracy of the nano-patterns are affected by the nanoimprinting temperature. The maximum depth of the nano-pattern could be achieved at 150 K, whereas the minimum depth could be obtained at 600 K. In contrast, the maximum width of the nano-pattern is attained at 600 K, while the minimum width is observed at 150 K. It is found that the best morphological accuracy can be achieved at the nanoimprinting temperature of 450 K.
- (5) The surface pile-up demonstrates a significant increasing trend with the elevated nanoimprinting temperature during the nanoimprinting process, while the impact of increased pressing speed on the surface pile-up is minimal.

Yi Zhang: Conceptualization, Investigation, Methodology, Software, Data curation, Formal analysis, Writing—original draft preparation. **Qianhao Xiao** and **Yunlong Han:** Data curation, Formal analysis. **Wenbo Zhang:** Supervision, Project administration. **Xichun Luo:** Investigation, Methodology, Software. **Jining Sun** and **Lei Zhang:** Conceptualization, Investigation, Methodology, Writing—review and editing, Supervision, Project administration, Funding acquisition.

Declaration of Competing Interest

The authors declare that they have no known competing financial interests or personal relationships that could have appeared to influence the work reported in this paper.

Data availability

Data will be made available on request.

Acknowledgments

The authors would like to thank the startup funding support by the Dalian University of Technology (DUT) (award no. 82232022, 82232043, and DUT22LAB404).

References

- [1] K.S. Cho, P. Mandal, K. Kim, I.H. Baek, S. Lee, H. Lim, D.J. Cho, S. Kim, J. Lee, F. Rotermund, Improved efficiency in GaAs solar cells by 1D and 2D nanopatterns fabricated by laser interference lithography, *Opt. Commun.* 284 (2011) 2608–2612. <https://doi.org/10.1016/j.optcom.2011.01.042>.
- [2] J.S. Mangum, S. Theingi, M.A. Steiner, W.E. McMahon, E.L. Warren, Development of High-Efficiency GaAs Solar Cells Grown on Nanopatterned GaAs Substrates, *Cryst. Growth Des.* 21 (2021) 5955–5960. <https://doi.org/10.1021/acs.cgd.1c00835>.
- [3] J. Tommila, A. Tukiainen, J. Viheriälä, A. Schramm, T. Hakkarainen, A. Aho, P. Stenberg, M. Dumitrescu, M. Guina, Nanoimprint lithography patterned GaAs templates for site-controlled InAs quantum dots, *J. Cryst. Growth.* 323 (2011) 183–186. <https://doi.org/10.1016/j.jcrysgro.2010.11.165>.

- [4] H. Kim, J. Choi, Z. Lingley, M. Brodie, Y. Sin, T.F. Kuech, P. Gopalan, L.J. Mawst, Selective growth of strained (In)GaAs quantum dots on GaAs substrates employing diblock copolymer lithography nanopatterning, *J. Cryst. Growth* 465 (2017) 48–54. <https://doi.org/10.1016/j.jcrysgro.2017.02.046>.
- [5] Y. Diao, L. Liu, S. Xia, Exploration the p-type doping mechanism of GaAs nanowires from first-principles study, *Phys. Lett. A* 383 (2019) 202–209. <https://doi.org/10.1016/j.physleta.2018.10.037>.
- [6] P.D. Ye, G.D. Wilk, E.E. Tois, J.J. Wang, Formation and characterization of nanometer scale metal-oxide-semiconductor structures on GaAs using low-temperature atomic layer deposition, *Appl. Phys. Lett.* 87 (2005) 013501. <https://doi.org/10.1063/1.1954902>.
- [7] S.H. Ko, I. Park, H. Pan, C.P. Grigoropoulos, A.P. Pisano, C.K. Luscombe, J.M.J. Fréchet, Direct nanoimprinting of metal nanoparticles for nanoscale electronics fabrication, *Nano Lett.* 7 (2007) 1869–1877. <https://doi.org/10.1021/nl070333v>.
- [8] Q.C. Hsu, C.D. Wu, T.H. Fang, Studies on nanoimprint process parameters of copper by molecular dynamics analysis, *Computational Materials Science* 34 (2005) 314–322. <https://doi.org/10.1016/j.commatsci.2005.01.004>.
- [9] L.R. Bao, X. Cheng, X.D. Huang, L.J. Guo, S.W. Pang, A.F. Yee, Nanoimprinting over topography and multilayer three-dimensional printing, *Journal of Vacuum Science & Technology B: Microelectronics and Nanometer Structures Processing, Measurement, and Phenomena.* 20 (2002) 2881–2886. <https://doi.org/10.1116/1.1526355>.
- [10] L.J. Guo, Nanoimprint lithography: methods and material requirements, *Adv. Mater.* 19 (2007) 495–513. <https://doi.org/10.1002/adma.200600882>.
- [11] K. Nishio, K. Yasui, F. Matsumoto, K. Kanezawa, H. Masuda, Direct Nanoimprinting of Si Single Crystals Using SiC Molds for Ordered Anodic Tunnel Etching, *Advanced Materials* 17 (2005) 1293–1295. <https://doi.org/10.1002/adma.200401879>.
- [12] B. Zhang, H. Yang, C. Pan, P. Zhao, Joint process of laser shock polishing and imprinting for metallic nanostructure fabrication, *Mater. Des.* 227 (2023) 111743. <https://doi.org/10.1016/j.matdes.2023.111743>.
- [13] B.T. Sayed, M.M. Al-Sakhnini, Asaad.A.H. Alzubaidi, A.H.R. Alawadi, A.J. Ibrahim, S. Askar, Assessment of Nano-Imprinting Process in CuZr Amorphous Films Through Combination of Machine Learning and Molecular Dynamics, *J. Electron. Mater.* 52 (2023) 6943–6958. <https://doi.org/10.1007/s11664-023-10630-4>.
- [14] D.L. Chen, T.C. Chen, Mechanical properties of Au nanowires under uniaxial tension with high strain-rate by molecular dynamics, *Nanotechnology.* 16 (2005) 2972–2981. <https://doi.org/10.1088/0957-4484/16/12/041>.
- [15] T.H. Fang, W.J. Chang, S.L. Lin, Effects of temperature and speed of droplet ejection process of simulated nanojets onto a moving plate's surface, *Appl. Surf. Sci.* 253 (2006) 1649–1654. <https://doi.org/10.1016/j.apsusc.2006.02.062>.
- [16] W.J. Chang, T.-H. Fang, Influence of temperature on tensile and fatigue behavior of nanoscale copper using molecular dynamics simulation, *J. Phys. Chem. Solids.* 64 (2003) 1279–1283. [https://doi.org/10.1016/S0022-3697\(03\)00130-6](https://doi.org/10.1016/S0022-3697(03)00130-6).
- [17] C.H. Wang, K.C. Chao, T.H. Fang, I. Stachiv, S.F. Hsieh, Investigations of the mechanical properties of nanoimprinted amorphous Ni–Zr alloys utilizing the molecular dynamics simulation, *J. Alloys Compd.* 659 (2016) 224–231. <https://doi.org/10.1016/j.jallcom.2015.11.068>.
- [18] J.H. Kang, K.S. Kim, K.W. Kim, Molecular dynamics study on the effects of stamp shape, adhesive energy, and temperature on the nanoimprint lithography process, *Appl. Surf. Sci.* 257 (2010) 1562–1572. <https://doi.org/10.1016/j.apsusc.2010.08.096>.
- [19] V.T. Nguyen, T.H. Fang, Temperature and vibration-assisted effects in nanoimprint gold: An atomistic study, *Mater. Chem. Phys.* 292 (2022) 126832. <https://doi.org/10.1016/j.matchemphys.2022.126832>.

- [20] T.H. Fang, C.D. Wu, W.J. Chang, S.S. Chi, Effect of thermal annealing on nanoimprinted Cu–Ni alloys using molecular dynamics simulation, *Appl. Surf. Sci.* 255 (2009) 6043–6047. <https://doi.org/10.1016/j.apsusc.2009.01.069>.
- [21] S. Park, Z. Song, L. Brumfield, A. Amirsadeghi, J. Lee, Demolding temperature in thermal nanoimprint lithography, *Appl. Phys. A*. 97 (2009) 395–402. <https://doi.org/10.1007/s00339-009-5224-0>.
- [22] M. Koyama, M. Shirai, H. Kawata, Y. Hirai, M. Yasuda, Stochastic simulation of the UV curing process in nanoimprint lithography: Pattern size and shape effects in sub-50 nm lithography, *Journal of Vacuum Science & Technology B, Nanotechnology and Microelectronics: Materials, Processing, Measurement, and Phenomena*. 35 (2017) 06G307. <https://doi.org/10.1116/1.4997295>.
- [23] Q.X. Pei, C. Lu, Z.S. Liu, K.Y. Lam, Molecular dynamics study on the nanoimprint of copper, *J. Phys. D: Appl. Phys.* 40 (2007) 4928. <https://doi.org/10.1088/0022-3727/40/16/026>.
- [24] Z. Zhu, T. Zhou, Y. He, Q. Yu, X. Wang, T. Yan, J. Yan, H. Ruan, Antireflective structured surface of chalcogenide glass fabricated using glass to glass molding, *Ceram. Int.* 49 (2023) 28216–28223. <https://doi.org/10.1016/j.ceramint.2023.06.076>.
- [25] T.W. Besar Riyadi, R. Sivaraman, A.M. Hussein Wais, F.M.A. Altalbawy, U.O. Khudanov, D.K. Chaudhary, Mechanism of Imprinting Process in the Ni-P Metallic Glass Films: A Molecular Dynamics Study, *Adv. Mater. Sci. Eng.* 2023 (2023) 1–8. <https://doi.org/10.1155/2023/6232579>.
- [26] V.-T. Pham, T.-N. Vu, D.-B. Luu, V.-T. Hoang, Q.-B. Tao, Effects of temperature, punch angle, and loading velocity on mechanical properties of nanoimprinted FeNiCoCrCu_x high-entropy alloys, *Mater. Today Commun.* 38 (2024) 107692. <https://doi.org/10.1016/j.mtcomm.2023.107692>.
- [27] C. Chen, M. Lai, F. Fang, Study on the crack formation mechanism in nano-cutting of gallium arsenide, *Appl. Surf. Sci.* 540 (2021) 148322. <https://doi.org/10.1016/j.apsusc.2020.148322>.
- [28] S. Plimpton, Fast Parallel algorithms for short-range molecular dynamics, *J. Comput. Phys.* 117 (1995) 1–19. <https://doi.org/10.1006/jcph.1995.1039>.
- [29] P. Fan, F. Ding, X. Luo, Y. Yan, Y. Geng, Y. Wang, A simulated investigation of ductile response of GaAs in single-point diamond turning and experimental validation, *Nanomanufacturing and Metrology*. 3 (2020) 239–250. <https://doi.org/10.1007/s41871-020-00080-5>.
- [30] P. Fan, S. Goel, X. Luo, Y. Yan, Y. Geng, Y. He, Y. Wang, Molecular dynamics simulation of AFM tip-based hot scratching of nanocrystalline GaAs, *Mater. Sci. Semicond. Process.* 130 (2021) 105832. <https://doi.org/10.1016/j.mssp.2021.105832>.
- [31] I. Štich, R. Car, M. Parrinello, S. Baroni, Conjugate gradient minimization of the energy functional: A new method for electronic structure calculation, *Phys. Rev. B*. 39 (1989) 4997–5004. <https://doi.org/10.1103/PhysRevB.39.4997>.
- [32] L. Xue, G. Feng, S. Liu, Molecular dynamics study of temperature effect on deformation behavior of m-plane 4H–SiC film by nanoindentation, *Vacuum*. 202 (2022) 111192. <https://doi.org/10.1016/j.vacuum.2022.111192>.
- [33] S. Nosé, A unified formulation of the constant temperature molecular dynamics methods, *J. Chem. Phys.* 81 (1984) 511–519. <https://doi.org/10.1063/1.447334>.
- [34] P. Fan, N.K. Katiyar, S. Goel, Y. He, Y. Geng, Y. Yan, H. Mao, X. Luo, Oblique nanomachining of gallium arsenide explained using AFM experiments and MD simulations, *J. Manuf. Processes*. 90 (2023) 125–138. <https://doi.org/10.1016/j.jmapro.2023.01.002>.
- [35] P. Fan, S. Goel, X. Luo, Y. Yan, Y. Geng, Y. Wang, An atomistic investigation on the wear of diamond during atomic force microscope tip-based nanomachining of gallium arsenide, *Comput. Mater. Sci.* 187 (2021) 110115. <https://doi.org/10.1016/j.commatsci.2020.110115>.

- [36] P. Fan, S. Goel, X. Luo, Y. Yan, Y. Geng, Y. He, Y. Wang, Molecular dynamics simulation of AFM tip-based hot scratching of nanocrystalline GaAs, *Mater. Sci. Semicond. Process.* 130 (2021) 105832. <https://doi.org/10.1016/j.mssp.2021.105832>.
- [37] A. Stukowski, Visualization and analysis of atomistic simulation data with OVITO—the Open Visualization Tool, *Model. Simul. Mater. Sci. Eng.* 18 (2010) 015012. <https://doi.org/10.1088/0965-0393/18/1/015012>.
- [38] A. Stukowski, K. Albe, Extracting dislocations and non-dislocation crystal defects from atomistic simulation data, *Model. Simul. Mater. Sci. Eng.* 18 (2010) 085001. <https://doi.org/10.1088/0965-0393/18/8/085001>.
- [39] A. Stukowski, V.V. Bulatov, A. Arsenlis, Automated identification and indexing of dislocations in crystal interfaces, *Model. Simul. Mater. Sci. Eng.* 20 (2012) 085007. <https://doi.org/10.1088/0965-0393/20/8/085007>.
- [40] S.Z. Chavoshi, S. Goel, X. Luo, Influence of temperature on the anisotropic cutting behaviour of single crystal silicon: A molecular dynamics simulation investigation, *J. Manuf. Processes.* 23 (2016) 201–210. <https://doi.org/10.1016/j.jmapro.2016.06.009>.
- [41] S. Goel, N.H. Faisal, V. Ratia, A. Agrawal, A. Stukowski, Atomistic investigation on the structure–property relationship during thermal spray nanoparticle impact, *Comput. Mater. Sci.* 84 (2014) 163–174. <https://doi.org/10.1016/j.commatsci.2013.12.011>.
- [42] J. Li, Q. Fang, B. Liu, Y. Liu, Y. Liu, Atomic-scale analysis of nanoindentation behavior of high-entropy alloy, *Journal of Micromechanics and Molecular Physics.* 01 (2016) 1650001. <https://doi.org/10.1142/S2424913016500016>.
- [43] S. Goel, X. Luo, R.L. Reuben, Shear instability of nanocrystalline silicon carbide during nanometric cutting, *Appl. Phys. Lett.* 100 (2012) 231902. <https://doi.org/10.1063/1.4726036>.
- [44] J. Rong, P. Zhu, Study on wear of diamond during scratching SiC using molecular dynamics simulations, *Mater. Today Commun.* 38 (2024) 108448. <https://doi.org/10.1016/j.mtcomm.2024.108448>.
- [45] F. Shimizu, S. Ogata, J. Li, Theory of shear banding in metallic glasses and molecular dynamics calculations, *Mater. Trans.* 48 (2007) 2923–2927. <https://doi.org/10.2320/matertrans.MJ200769>.
- [46] W.C. Oliver, G.M. Pharr, An improved technique for determining hardness and elastic modulus using load and displacement sensing indentation experiments, *J. Mater. Res.* 7 (1992) 1564–1583. <https://doi.org/10.1557/JMR.1992.1564>.
- [47] C.D. Wu, T.H. Fang, P.H. Sung, Q.C. Hsu, Critical size, recovery, and mechanical property of nanoimprinted Ni–Al alloys investigation using molecular dynamics simulation, *Comput. Mater. Sci.* 53 (2012) 321–328. <https://doi.org/10.1016/j.commatsci.2011.09.027>.
- [48] D.Q. Doan, T.H. Fang, A.S. Tran, T.H. Chen, Residual stress and elastic recovery of imprinted Cu-Zr metallic glass films using molecular dynamic simulation, *Comput. Mater. Sci.* 170 (2019) 109162. <https://doi.org/10.1016/j.commatsci.2019.109162>.
- [49] A.V. Pham, T.H. Fang, V.T. Nguyen, T.H. Chen, Mechanical characteristics of Ni₅₀Co₅₀/Ni substrate during indentation by molecular dynamics, *Model. Simul. Mater. Sci. Eng.* 30 (2022) 045006. <https://doi.org/10.1088/1361-651X/ac5c65>.
- [50] C.R. Das, S. Dhara, Y.-R. Jeng, P.-C. Tsai, H.C. Hsu, B. Raj, A.K. Bhaduri, S.K. Albert, A.K. Tyagi, L.C. Chen, K.H. Chen, Direct observation of amorphization in load rate dependent nanoindentation studies of crystalline Si, *Appl. Phys. Lett.* 96 (2010) 253113. <https://doi.org/10.1063/1.3456380>.
- [51] K.E. Avila, V.H. Vardanyan, S. Kuchemann, H.M. Urbassek, Response of an amorphous/crystalline interface to nanoindentation: an atomistic study, *Appl. Surf. Sci.* 551 (2021) 149285. <https://doi.org/10.1016/j.apsusc.2021.149285>.
- [52] K.E. Avila, S. Kuchemann, H.M. Urbassek, Structure and size of the plastic zone formed during nanoindentation of a metallic glass, *J. Non-Cryst. Solids* 523 (2019) 119593. <https://doi.org/10.1016/j.jnoncrysol.2019.119593>.

- [53] C. Liu, A. Das, W. Wang, S. Küchemann, P. Kenesei, R. Maaß, Shear-band cavities and strain hardening in a metallic glass revealed with phase-contrast x-ray tomography, *Scr. Mater.* 170 (2019) 29–33. <https://doi.org/10.1016/j.scriptamat.2019.05.021>.
- [54] C. Chen, M. Lai, F. Fang, Subsurface deformation mechanism in nano-cutting of gallium arsenide using molecular dynamics simulation, *Nanoscale Res. Lett.* 16 (2021) 117. <https://doi.org/10.1186/s11671-021-03574-3>.
- [55] J.M. Haile, I. Johnston, A.J. Mallinckrodt, S. McKay, Molecular dynamics simulation: elementary methods, *Computer in Physics* 7 (1993) 625. <https://doi.org/10.1063/1.4823234>.
- [56] J. Guo, J. Chen, Y. Wang, Temperature effect on the mechanical response of c-plane monocrystalline gallium nitride in nanoindentation: A molecular dynamics study, *Ceram. Int.* 46 (2020) 12686–12694. <https://doi.org/10.1016/j.ceramint.2020.02.035>.
- [57] Y. Wang, J. Shi, Phase transformation of monocrystalline silicon by nanoindentation – Effect of processing temperature, *Mater. Sci. Semicond. Process.* 102 (2019) 104601. <https://doi.org/10.1016/j.mssp.2019.104601>.

Author contributions:

Yi Zhang: Conceptualization, Investigation, Methodology, Software, Data curation, Formal analysis, Writing—original draft preparation; Qianhao Xiao and Yunlong Han: Data curation, Formal analysis; Wenbo Zhang: Supervision, Project administration; Xichun Luo: Investigation, Methodology, Software; Jining Sun and Lei Zhang: Conceptualization, Investigation, Methodology, Writing—review and editing, Supervision, Project administration, Funding acquisition.

Declaration of interests

The authors declare that they have no known competing financial interests or personal relationships that could have appeared to influence the work reported in this paper.